

Article

Two-Sided Surface Oxidized Cellulose Membranes Modified with PEI: Preparation, Characterization and Application for Dyes Removal

Wei Wang *, Qian Bai, Tao Liang, Huiyu Bai and Xiaoya Liu

Key Laboratory of Synthetic and Biological Colloids, Ministry of Education, School of Chemical and Material Engineering, Jiangnan University, Wuxi 214122, China; qianbaichem@163.com (Q.B.); taoliangchem@163.com (T.L.); bhy.chem@163.com (H.B.); lxy@jiangnan.edu.cn (X.L.)

* Correspondence: ww12230098@sina.com or weiwangpolymer@163.com

Received: 16 August 2017; Accepted: 13 September 2017; Published: 16 September 2017

Abstract: Porous regenerated cellulose (RC) membranes were prepared with cotton linter pulp as a raw material. These membranes were first oxidized on both sides by a modified (2,2,6,6-tetramethylpiperidin-1-yl)oxyl (TEMPO) oxidation system using a controlled oxidation reaction technique. Then, the oxidized RC membranes were functionalized with polyethylenimine (PEI) via the glutaraldehyde crosslinking method to obtain bifunctional (carboxyl and amino) porous RC membranes, as revealed by Fourier transform infrared spectroscopy (FT-IR), elemental analysis and zeta potential measurement. The scanning electron microscopy (SEM) and the tests of the mechanical properties and permeability characteristics of modified RC membranes demonstrated that the porous structure and certain mechanical properties could be retained. The adsorption performance of the modified membranes towards dyes was subsequently investigated. The modified membranes displayed good adsorption capacities, rapid adsorption equilibrium and removal efficiencies towards both anionic (xylenol orange (XO)) and cationic (methylene blue (MB)) dyes, making them suitable bioadsorbents for wastewater treatment.

Keywords: regenerated celluloses; bioadsorbents; dye removal; functional membranes

1. Introduction

Synthetic dyes are widely utilized in numerous industries (e.g., textile, paper, leather tanning, plastics, rubber, cosmetics and printing) owing to their high stability, relatively low costs and color uniformity characteristics [1,2]. Inevitably, a certain fraction of dyes end up in the effluent during the dyeing process. This colored waste water must be purified before being released into the environment since it is toxic, carcinogen and can damage the aquatic ecological balance [3]. Various methods (e.g., adsorption, membrane separation, chemical oxidation, coagulation-flocculation, photochemical degradation and bioremoval) have been used singly or in combination with other approaches for the removal of dyes [4–6]. Among them, adsorption is considered to be economically and environmentally superior to other conventional techniques owing to its easy operation, low cost and effectiveness [7]. However, mechanical agitation is often required to improve the adsorption efficiency by enhancing the contact between the dyes and the adsorbents. Moreover, numerous adsorbents usually require long times before reaching adsorption equilibrium [8].

One paradigmatic adsorbent for the removal of a target pollutant should exhibit a large surface area, good adsorption efficiency and an abundance of adsorption sites while being produced at low cost and in a sustainable and environmentally-friendly manner. Sharma et al. compiled a list of naturally available, low cost and eco-friendly adsorbents for the removal of hazardous dyes from aqueous

waste streams via adsorption [4]. Various methods including carbonization, chemical activation and pyrolysis have been proposed to enhance the adsorption efficiency for dyes [9].

Biodegradable and biocompatible cellulose-based materials have been developed in recent decades taking advantage of the wide availability (i.e., the most abundant renewable biopolymer in nature) and low cost characteristics of this polymer. These materials have been used for water treatment purposes especially, as a new class of versatile adsorbents for the removal of dyes. Moreover, the high density of surface hydroxyl groups present on cellulose provides this material with excellent surface modification characteristics, thereby allowing a wide range of functionalization approaches for the adsorption of dyes from aqueous solutions [10]. Thus, different forms of cellulose-based materials have been used as dye adsorbents. Jin et al. prepared amino-functionalized nanocrystalline cellulose, and the sample was then applied as an adsorbent to remove anionic dyes in aqueous solutions [11]. A carboxylate-functionalized adsorbent based on CNCs was prepared, and adsorptive removal of multiple cationic dyes was investigated [12]. Cellulose recycled newspaper fibers were grafted with double quaternary ammonium groups, and the maximum adsorption capacity of this for RTB G-133 was $524 \text{ mg}\cdot\text{g}^{-1}$ [13]. Luo et al. developed millimeter-scale magnetic regenerated cellulose (RC) beads, and the adsorbent could efficiently adsorb the organic dyes from wastewater, as well as the used adsorbents could be recovered completely [14]. Cellulose nanosponges modified with methyltrioctylammonium chloride were prepared and used for pre-concentration, removal and determination of tartrazine dye, using UV-Vis spectrophotometry [15]. Cellulose powders functionalized with hyperbranched polyethylenimine were prepared, and used for selective dye adsorption and separation based on the unique selective adsorption [16].

Cellulose membranes can be also used as dye adsorbents, benefitting from the porous structure, the adsorption capacity for the removal of positively-charged dyes and good reusable performance, however in the form of multilayer [17], composites [18,19] and cellulose derivatives [20]. However, at present, many studies have focused on using membrane separation technology as the cellulose-based membranes are used for water treatment [21,22], and there are less reports on the pure cellulose functional membranes as adsorbents. Oshima et al., reported phosphorylated bacterial cellulose as an adsorbent for metal ions [23]. As described above, when used as adsorbents, celluloses need to undergo chemical modification for achieving efficient adsorption. However, during the modification process, celluloses are often subjected to strong acid or oxidant, etc., treatments, so leading to the degradation of cellulose macromolecules [24], which further may damage the porous structures of the cellulose membranes and even destroy membranes themselves. These facts can significantly limit the application of cellulose membranes for adsorption purposes.

In this study, cotton linter pulp was used as a raw material to prepare porous RC membranes by using a phase-inversion method. Subsequently, the RC membranes underwent a two-sided surface oxidation treatment with a modified (2,2,6,6-tetramethylpiperidin-1-yl)oxyl (TEMPO) oxidation system to yield the corresponding C-6 carboxyl membrane materials. To prevent the cellulose membranes from being damaged via oxidation-degradation of the cellulose macromolecular chains, a control oxidation reaction was carried out by following the method described by Fitz-Binder et al. [25]. Amine groups were subsequently incorporated onto the oxidized cellulose membranes by grafting polyethylenimine (PEI) via the glutaraldehyde crosslinking method [26]. As a result, porous RC membranes containing both carboxyl and amino groups were obtained. Fourier transform infrared spectroscopy (FT-IR), elemental analysis and zeta potential measurement and scanning electron microscopy (SEM) were used to analyze the structure and morphology of the modified cellulose membranes. Furthermore, anionic and cationic dyes were both used as model pollutants to evaluate the dye removal efficiency of the modified cellulose membranes. The adsorption performance and kinetic behaviors during dye adsorption on the cellulose-based adsorbents were further investigated. With the aim to further evaluate the potential application of the modified RC membranes for water treatment purposes, the porosity, pure water permeability characteristics and the mechanical properties of the modified RC membranes were also tested.

2. Experimental Section

2.1. Materials

Cellulose (cotton linter pulp, α -cellulose $\geq 95\%$) was purchased from Hubei Chemical Fiber Group Ltd. (Xiangfan, China). PEI (molecular weight of 600 Da), TEMPO (AR), xylene orange (XO) (AR) and methylene blue (MB) (AR) were supplied by Aladdin Chemical Reagent Corp., Shanghai, China. Other reagents used in this work were of analytical grade and purchased from Sinopharm Chemical Reagent Co., Shanghai, China.

2.2. Preparation of the RC Membranes

RC membranes were prepared according to a reported method [27]. Five grams of cotton linter pulp were added to a LiOH/urea/H₂O (8.76/12/79.24 in wt %, 100 g) solution, and the resulting aqueous solution was stored at 200 °C for 20 h. The frozen cellulose solution was then vigorously stirred for 5 min at ambient temperature to obtain a transparent cellulose dope. The cellulose dope was then subjected to centrifugation at 8000 rpm for 10 min at -4 °C, and the transparent supernatant fraction was immediately cast on a glass plate. Subsequently, the resulting gel sheets were coagulated with a sulfate aqueous solution to obtain a transparent membrane. The wet membrane was washed with deionized water and dried at ambient temperature to finally obtain the RC membrane.

2.3. Preparation of the TEMPO-Oxidized RC Membranes

Oxidized cellulose membranes were prepared according to a reported method [25]. First, the RC membrane was immersed in 1 L of a boric acid (0.1 M) buffer solution (pH = 10.5), and 2 g of NaBr and 0.3 g of TEMPO were subsequently added and mixed by magnetic stirring for 180 min. The pre-wetted membranes were then dried at 60 °C for 5 min. For the printing paste, 5 g of alginate were dissolved in 40 mL of the boric acid buffer solution to form a thickener, and 6 mL of NaOCl were added to the former paste. The mixtures were then stirred to obtain a homogenous paste. Subsequently, the as-prepared thickener paste was applied by printing it on the one-sided surface of the RC membranes containing the NaBr/TEMPO/buffer mixture, and the prints were rested for 60 min. Finally, the printing membrane was thoroughly washed with water. The other side of the cellulose membrane was impregnated in a similar way to generate the two-sided surface TEMPO-oxidized regenerated cellulose (TORC) membrane.

2.4. Preparation of Aminated TORC Membranes

The oxidized RC membranes were cut into approximately 80 mm \times 70 mm \times 0.1 mm pieces and saturated in 50 mL of an anhydrous methanol solution. Four grams of PEI were added, and the resulting solution was stirred at room temperature for 24 h. After that, the wet membranes were rinsed with water to remove the residual PEI and immediately immersed in 100 mL of an anhydrous methanol solution. Subsequently, 20 mL of a glutaraldehyde solution were added dropwise, and the resultant mixtures were stirred at 25 °C for 2 h. Finally, the modified cellulose membranes were repeatedly washed with deionized water to remove the unreacted material and denoted as PEI-TORC membranes.

2.5. Characterization of the Functionalized TORC Membranes

The RC and modified RC membranes were chemically characterized by attenuated total reflectance infrared (ATR-IR) spectroscopy (Nicolet 560, Nicolet Co., Ltd., Madison, WI, USA). The spectra were recorded from 600–4000 cm⁻¹ with a resolution of 2 cm⁻¹ and a minimum of 16 scans. The mass ratios of C, H, O and N of each sample were measured using Elemental Analyzer (Vario EL III, Elementar Co., Langensfeld, Germany). The surface and cross-section morphologies of the RC and modified RC membranes were assessed by using a scanning electron microscope (S-4800, Hitachi Corporation, Tokyo, Japan). Cross-sectional faces of membranes were prepared by being fractured in liquid nitrogen.

The samples were deposited on a glass plate and coated with a thin layer of gold/palladium using a sputter coater (K550X, Emitech Ltd., Kent, UK). The pore size analysis of the membrane surface was calculated by using the software of SEM image analysis (Nano Measurer System, Version 1.2.5, Fudan University, Shanghai, China). The surface charge of the PEI-TORC membrane was determined by zeta-potential measurement using an Electrokinetic Analyzer (SurPASS, Anton Paar, Graz, Austria), using a 2 mM KCl electrolyte solution. The tensile strength and strain at break of the membranes were measured on a universal testing machine (Instron 5967, Instron, Norwood, MA, USA), using a 250-N load cell at room temperature. The strain rate was set at 10 mm/min, and five measurements were taken for each sample.

The porosities of the modified membranes were calculated using a reported method [22]. The porosity (P) was calculated as Equation (1):

$$P = \frac{(M_1 - M_2)/q_1}{(M_1 - M_2)/q_1 + M_2/q_2} \times 100\% \quad (1)$$

The wet membranes were weighed as M_1 and then freeze dried overnight and weighed as M_2 . The water content was calculated as $M_1 - M_2$. q_1 is water density, and q_2 is PEI-TORC density (calculated according to the density of bulk cellulose, 1.5 g cm^{-3}).

The water flux of the modified membranes was evaluated using a reported method [28]. The pure water permeability test of the wet membranes was carried out on miniature microfiltration equipment at ambient temperature under an operation pressure of 0.1 MPa, while the water flux was calculated according to Equation (2):

$$J_w = \frac{V}{S \times t \times P} \quad (2)$$

where V is the volume of solvent passing through the membrane; t is the measurement time; S is the effective membrane area; P is the pressure (0.1 MPa).

The mean pore radius, r_f , was calculated by employing Equation (3), derived based on the straight-through cylindrical pore model [29].

$$\eta = \sqrt{\frac{8 \times \eta \times I \times J}{P \times \Delta P}} \quad (3)$$

where η is the water viscosity ($8.9 \times 10^{-4} \text{ Pa s}$), I is the membrane thickness (m), J is the permeation flux ($\text{m}^3 \cdot \text{m}^{-2} \cdot \text{s}^{-1}$) and ΔP is the load pressure (Pa).

2.6. Batch Adsorption Experiments

Batch adsorption experiments were conducted in some 100 mL glass conical flasks in a water bath shaker (25 °C, 200 rpm). Each flask contained 60 mL MB or XO solution and 70 mg adsorbent. The pH of the solution was adjusted by adding 0.1 M HCl or NaOH aqueous solutions. At predetermined time intervals, approximately 3 mL of dye solution were used for UV-Vis measurements and afterwards returned into the flask. This was repeated until equilibrium was reached. The dye removal efficiencies of the RC and PEI-TORC membranes towards XO and MB were investigated for 100 min (dye concentration, $30 \text{ mg} \cdot \text{L}^{-1}$, pH = 6.8). The effect of pH on the removal efficiency was investigated in the range of 4–11 for 100 min (dye concentration: $30 \text{ mg} \cdot \text{L}^{-1}$). The effect of initial dye concentration on the adsorption performance was investigated in the range from 30–1230 $\text{mg} \cdot \text{L}^{-1}$ (at pH values of 6.8 and 4.6) for 120 min. The effect of the contact time (10–100 min) was investigated (dye concentration, $30 \text{ mg} \cdot \text{L}^{-1}$) at pH 6.8 and 4.6.

The removal efficiency and adsorption capacity of dyes were calculated according to Equations (4) and (5):

$$\text{adsorption capacity (mg} \cdot \text{g}^{-1}) = \frac{(C_0 - C_t) \times V}{m} \times 100 \quad (4)$$

$$\text{Removal efficiency (\%)} = \frac{C_0 - C_t}{C_0} \times 100 \quad (5)$$

where C_0 ($\text{mg}\cdot\text{L}^{-1}$) and C_t ($\text{mg}\cdot\text{L}^{-1}$) are the initial concentration of the dye and the concentration of the dye at an adsorption time t , respectively, V is the volume of the dye solution and m is the weight of the adsorbent.

The evaluation of the reusability of the adsorbent was carried out at a $0.07 \text{ g}\cdot\text{L}^{-1}$ dosage of bioadsorbent added into 60 mL of $30 \text{ mg}\cdot\text{L}^{-1}$ dye solutions for 100 min, and then, the adsorbent was taken out from the solution. The desorption and regeneration of the used adsorbent was performed by immersing the adsorbent in 30 mL of a 0.1 M NaOH or HCl solution for 5 h at room temperature and subsequently washed using distilled water till neutral for the next adsorption. The generated adsorbent was used for another adsorption study in the subsequent cycles.

2.7. Adsorption Isotherm and Kinetic Model

The Langmuir and Freundlich models [30] can be used to describe the adsorption dynamic equilibrium process by Equations (6) and (7):

$$\frac{c_e}{q_e} = \frac{1}{k_1 q_{\max}} + \frac{c_e}{q_{\max}} \quad (6)$$

$$\ln q_e = \ln k_f + \frac{\ln c_e}{n} \quad (7)$$

where q_e ($\text{mg}\cdot\text{g}^{-1}$) is the equilibrium adsorption capacity, q_{\max} ($\text{mg}\cdot\text{g}^{-1}$) is the maximum adsorption capacity, C_e ($\text{mg}\cdot\text{L}^{-1}$) is the equilibrium concentration of free dye molecules in the solution ($\text{mg}\cdot\text{L}^{-1}$), K_1 is the Langmuir constant and K_f and $1/n$ are Freundlich constants.

In order to explore the adsorption mechanism of the rate limiting steps involved, the pseudo-first order and the pseudo-second order kinetic models [31] were used to study the type of adsorption and the adsorption mechanism. The first and second order rate equations can be expressed as Equations (8) and (9):

$$\log(q_e - q_t) = \log q_e - \frac{k_1 t}{2.303} \quad (8)$$

$$\frac{t}{q_t} = \frac{1}{k_2 q_e^2} + \frac{t}{q_e} \quad (9)$$

where q_e and q_t are the amounts of adsorbed dye per unit mass of adsorbent ($\text{mg}\cdot\text{g}^{-1}$) at equilibrium and a time t , respectively, and k_1 and k_2 are the first order and the pseudo-second order adsorption rate constants, respectively.

3. Results and Discussion

3.1. Characterization of the Modified RC Membranes

The FTIR spectra of the RC, TORC and PEI-TORC membranes are shown in Figure 1a. Compared with the unmodified RC, the FTIR spectra of the TORC membranes showed a new peak at 1736 cm^{-1} , which was attributed to the C=O stretching frequency of the carboxyl group [32], thereby revealing a successful TEMPO-oxidation process. In the case of the PEI-TORC membranes, new absorption bands were observed at ca. 1653 cm^{-1} corresponding to the C=N stretching vibration, which was formed in the glutaraldehyde crosslinking process. Three new peaks appeared in the $1600\text{--}1800\text{-cm}^{-1}$ region and were ascribed to the C=O stretching vibration of carboxyl groups (1736 cm^{-1}), the N-H bending vibration of secondary (1615 cm^{-1}) and primary (1564 cm^{-1}) amines [33,34]. Furthermore, the large enhancement of the C-C skeleton vibration at 1157 cm^{-1} and the presence of the C-H characteristic peaks at 2924 and 2849 cm^{-1} for the PEI-TORC membranes further demonstrated the successful crosslinking reaction.

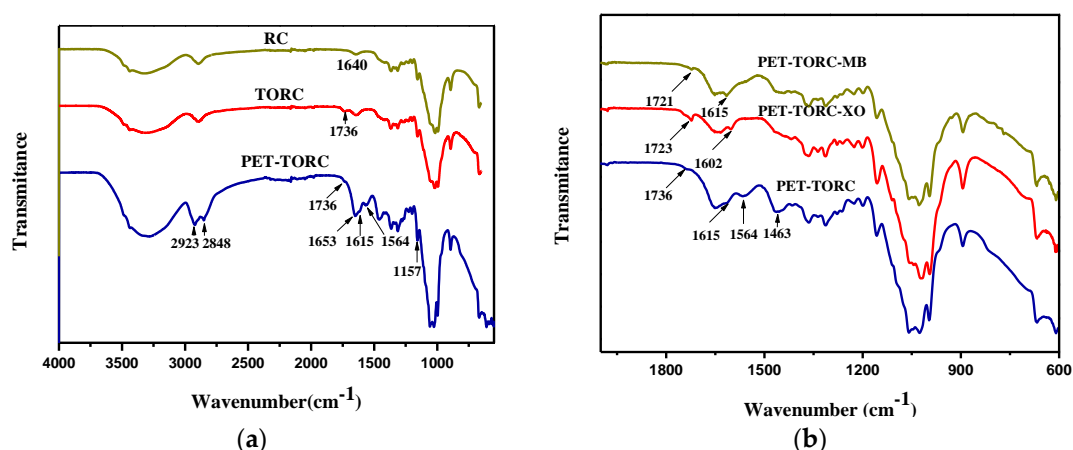


Figure 1. (a) FTIR spectra of RC, TORC, polyethylenimine(PEI)-(2,2,6,6-tetramethylpiperidin-1-yl)oxyl (TEMPO)-oxidized regenerated cellulose (TORC); (b) FTIR spectra of xylenol orange (XO)-adsorbed PEI-TORC and MB-adsorbed PEI-TORC.

In order to evaluate the change of the content of the elements in the whole material after modification, the contents of C, N, O and H in different cellulose-based membranes are listed in Table 1. After TEMPO oxidation, the oxygen content in cellulose increased from 49.11–51.29%. The nitrogen content of PEI-TORC increased significantly from 0–3.87% compared to that of TORC. The elemental analysis data and the FTIR results both confirmed the successful oxidation of cellulose and PEI grafting on TORC.

Table 1. Elements analysis results of unmodified and modified cellulose membranes.

Sample	C (%)	O (%)	H (%)	N (%)
RC	41.02	49.11	9.87	0
TORC	39.64	51.29	9.07	0
PEI-TORC	41.98	45.91	8.24	3.87

FT-IR is a useful tool to study the possible adsorbent-adsorbate interactions. The FT-IR spectra of the cellulose-based and the dye-loaded bioadsorbents are shown in Figure 1b. After dye adsorption, the adsorption peaks of the bioadsorbent shifted towards lower wavenumbers. For example, the adsorption peak attributed to the C=O stretching vibration shifted from 1736 to 1725 cm^{-1} (for XO) and 1724 cm^{-1} (for MB). The absorption bands assigned to the N–H stretching vibration shifted from 1615 to 1602 cm^{-1} (for XO) and 1613 cm^{-1} (for MB). After absorption, the disappearance of the N–H bending vibration peak of primary amines (1564 cm^{-1}) and the variation of the CH₂ bending peak (1463 cm^{-1}) also revealed the existence of electrostatic and hydrogen bonding interactions between the functional groups of the adsorbent and the dye molecules.

The SEM images for the RC, TORC and PEI-TORC membranes are shown in Figure 2. Surface morphology changes of cellulose-based membranes were observed; the porous structure of RC was maintained after TEMPO oxidation and crosslinking reaction. The average diameter of the pores of the pure cellulose membrane surface from SEM (78 nm, standard deviation of 18) was larger than that of PEI-TORC (43 nm, standard deviation of 10), revealing the reaction on the surface of the cellulose, introducing new groups and molecular chains on the membrane surface. As shown in the SEM images of the cross-section of cellulose-based membranes, compared with the cross-section morphology of RC membranes, the interior structures of TORC and PEI-TORC membranes had changed greatly. The cross-section of the RC membrane was relatively smooth. Interestingly, it can be observed that the cross-section image of the TORC membrane shows a non-homogeneous structure. This is because the control oxidation reaction leads to the fact that the pore structure and the microstructure of the

material are different between the surface and the interior of the TORC membrane. When fractured in liquid nitrogen, there is a different morphology from the homogeneous RC membrane. Compared with the cross-section morphology of PET-TORC membranes, the cross-section of the PEI-TORC membrane became flat, suggesting that the uniformity of the membrane structure was improved due to the crosslinking reaction; however, the pore size and shape of the middle part of the membrane are different from those of the peripheral part, suggesting both oxidation and crosslinking reaction affected the morphology and structure of the PEI-TORC membranes. Moreover, this structural feature makes it unsuitable as a molecular sieve.

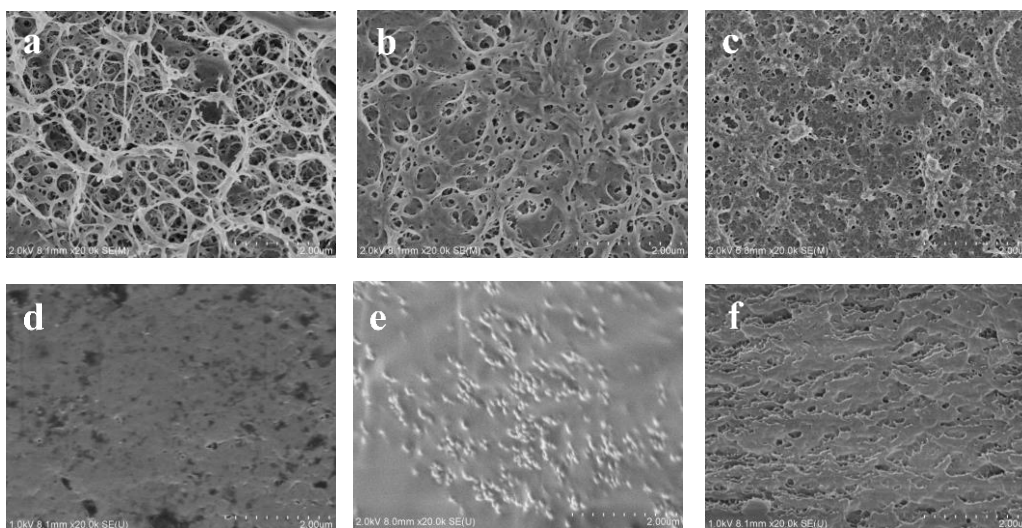


Figure 2. SEM images of the RC membrane: (a) surface, (d) cross-section; TORC membrane: (b) surface, (e) cross-section; PEI-TORC membrane: (c) surface, (f) cross-section.

As shown in Figure 3, the mechanical properties of the modified membranes were reduced. The tensile strength and elongation at break of RC membranes were 81.9 MPa, and 9.0%, respectively, while the tensile strength and elongation at break of PEI-TORC membranes were 31.0 MPa and 2.7%, respectively. The decrease of the mechanical properties of TORC membranes was due to the oxidative degradation of cellulose and the non-uniformity of the membrane materials caused by the control of the oxidation reaction. The decrease in elongation at break of the PEI-TORC membranes was due to the fact that the crosslinking reaction limits the movement of the molecular chain, and the descent in the tensile strength is likely due to the inhomogeneity of the material.

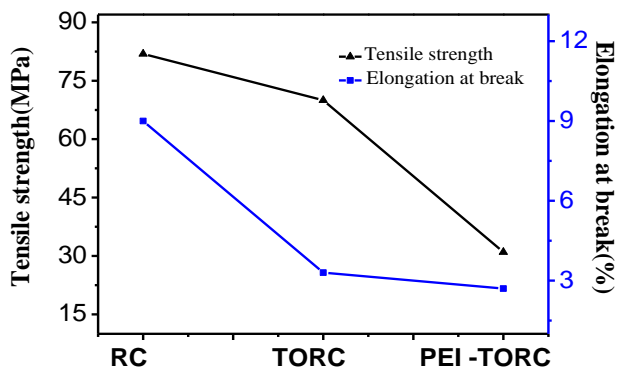


Figure 3. Tensile strength and elongation at break of RC, TORC and PEI-TORC membranes.

In order to explore the potential application value of membrane in water treatment, the structure and performance of the PEI-TORC membrane were further studied. The porosity, water flux and pore size of the PEI-TORC membrane were 72%, $6.14 \text{ L}\cdot\text{m}^{-2}\cdot\text{h}^{-1}\cdot\text{bar}^{-1}$ and 25.9 nm (the mean pore size), respectively. Importantly, it is possible to adjust the morphology, structure and properties of the PEI-TORC membrane by changing the various influencing factors in the preparation process, making it possible to further expand the application range of the modified cellulose membrane.

3.2. Adsorption Properties of the RC and PEI-TORC Membranes

The dye removal percentages of the RC and PEI-TORC membranes are also shown in Figure 4. RC membranes exhibited a poor adsorption capacity, meaning that raw cellulose did not have enough binding sites for dye adsorption. However, the adsorption capacity of hydroxyl for the removal of positively-charged dyes, the hydroxyl groups on the surface, is quite limited because most of them are included in the intra- and inter-molecule hydrogen-bond network. The removal efficiency of the PEI-TORC membrane was significantly higher than that of the RC material. The sorption of dyes onto adsorbents may well include chemical sorption, which could greatly improve the adsorption capacity. From the change in the FTIR of the functions in PEI-TORC upon the adsorption of MB or XO, it is apparent that the adsorption process is likely to involve chemical sorption.

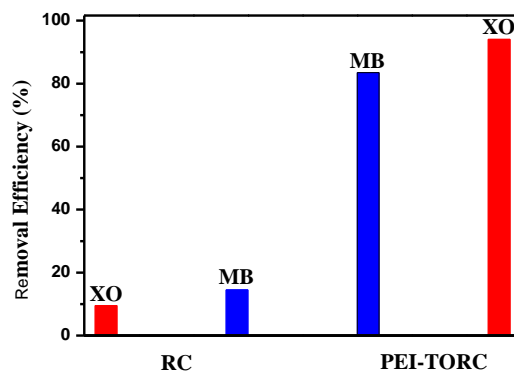


Figure 4. The removal efficiencies of RC and PEI-TORC (initial dye concentration: $30 \text{ mg}\cdot\text{L}^{-1}$, 60 mL MB or XO solution, 70 mg adsorbent, 100 min, pH = 6.8).

3.3. Effect of the pH on Adsorption

The solution pH significantly alters the level of electrostatic or molecular interaction between the adsorbent and the adsorbate due to the charge distribution on the material [11]. Thus, the pH of the solution is one of the determinants of the efficiency of the adsorbent for dye removal, as shown in Figure 5. The zeta potentials of PEI-TORC at various pH are also shown in Figure 5. The results showed that PEI-TORC exhibited a positively-charged surface at a pH lower than 5.7, while a negatively-charged surface at a pH higher than 5.7, which is shown to be electrically neutral (i.e., zero point charge). Xylenol orange is a negatively-charged species [35], while the methylene blue molecules are positively charged [36]. PEI-TORC exhibited positive surface charge at a pH lower than 5.7, leading to electrostatic attraction between the bioadsorbent and the anionic group of XO, resulting in maximum removal efficiency of 95.7% at pH 4.1. However, the PEI-TORC exhibited a negatively-charged surface, resulting in weaker electrostatic interactions between the bioadsorbent and XO and lower dye adsorption [37], with increasing the pH to higher than 5.7. The efficiency of the bioadsorbent for MB dye removal kept increasing in the pH range of 4.1–10.9, indicating the electronegativity of PEI-TORC continued to increase with increasing pH values. The results revealed the excellent dye removal efficiency of the bioadsorbent for both anionic and cationic dyes. The high adsorption of cationic or acidic dyes at higher pH may be due to the unique molecular structure of this

bioadsorbent. However, considering the practical application and the zeta potential of the adsorbent, this paper mainly studied the adsorption performance of the bioadsorbent at pH 4.6 and 6.8.

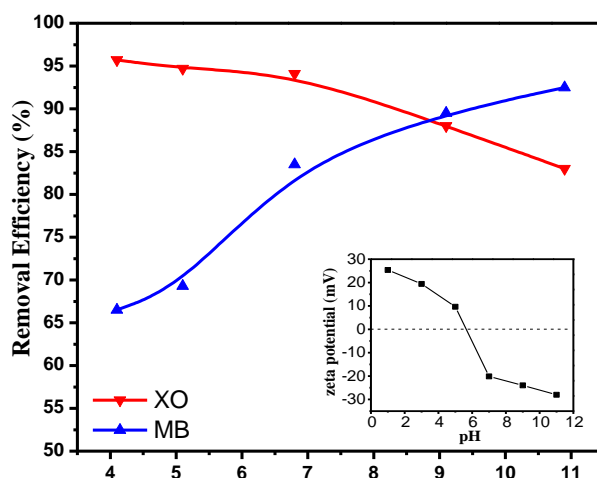


Figure 5. Effect of pH on the dye removal efficiencies of XO and MB (initial dye concentration: $200 \text{ mg}\cdot\text{L}^{-1}$, 30 mL dye solution, 70 mg adsorbent).

3.4. Effect of the Initial Dye Concentration and the Adsorption Isotherm

As shown in Figure 6a, the dye adsorption capacity of PEI-TORC increased with the increase of the initial concentration and then tended to level off, resulting from the increasing driving force from the concentration gradient [38]. However, the equilibrium adsorption capacity and the adsorption behavior of PET-TORC varied greatly due to different types of dyes and different pH values. The adsorption capacity of XO was higher than that of MB, which was attributed to the limited number of carboxyl groups on the surface of the bioadsorbent, caused by controlled oxidation. The maximum adsorption capacities of XO and MB reached 403 and $74 \text{ mg}\cdot\text{g}^{-1}$, at pH 4.6, respectively; while the maximum values of XO and MB reached 229 and $139 \text{ mg}\cdot\text{g}^{-1}$, at pH 6.8, respectively.

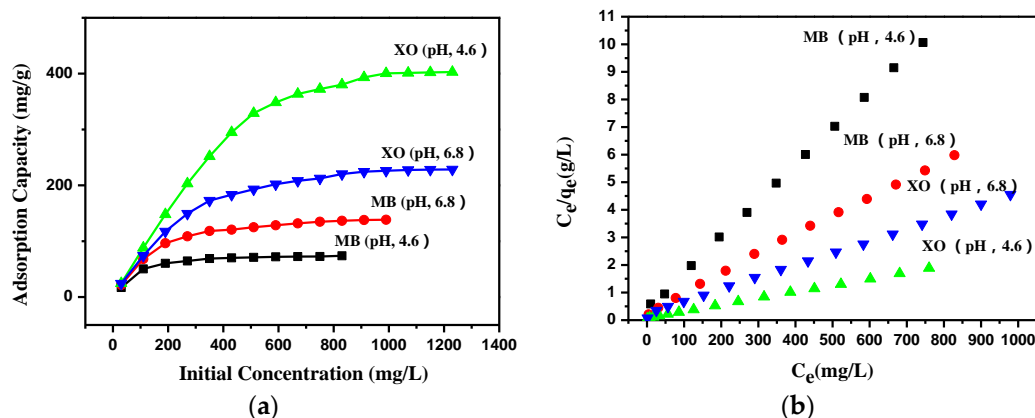


Figure 6. (a) Effect of initial concentration on dye adsorption by PEI-TORC membranes; (b) the plots of C_e/q_e against C_e for adsorption of XO and MB at different pH.

The adsorption isotherm study was carried out on two well-known isotherms, Langmuir and Freundlich. When C_e/q_e was plotted against C_e , a straight line with slope $1/q_{\text{max}}$ was obtained (Figure 6b), indicating that the adsorption of the both dyes onto PEI-TORC follows the Langmuir isotherm. The q_{max} values of the Langmuir model for adsorption of MB were $77 \text{ mg}\cdot\text{g}^{-1}$ (pH, 4.6) and $144 \text{ mg}\cdot\text{g}^{-1}$ (pH, 6.8), while the q_{max} values for adsorption of XO were $420 \text{ mg}\cdot\text{g}^{-1}$ (pH, 4.6) and

241 $\text{mg}\cdot\text{g}^{-1}$ (pH, 6.8), which was similar to the experimental q_{max} values obtained from Figure 6a. Thus, these results indicated that the PEI-TORC membrane exhibited relatively high effectiveness in removing the tested dyes, especially anionic dyes. Moreover, the isotherm parameters are summarized in Table 2. It is evident that the Langmuir isotherm model fits the experimental data better than the Freundlich model.

Table 2. Isotherm parameters for the adsorption of XO and MB onto PEI-TORC.

pH	Dyes	Langmuir Model			Freundlich Model		
		K_1 ($\text{L}\cdot\text{mg}^{-1}$)	q_{max} ($\text{mg}\cdot\text{g}^{-1}$)	R^2	n	K_f ($\text{mg}\cdot\text{g}^{-1}$)	R^2
6.8	XO	0.018	240.96	0.9981	2.89	25.28	0.9465
	MB	0.024	144.09	0.9987	3.12	18.64	0.8902
4.6	XO	0.030	420.17	0.9995	2.56	39.30	0.8922
	MB	0.031	76.57	0.9998	3.36	11.90	0.8170

3.5. Effect of the Contact Time and the Adsorption Kinetics

Figure 7 shows the dye removal efficiency and color change of XO and MB as a function of the adsorption time. The percentage of dye removal increased rapidly within the first 40 min, and the absorption equilibrium was reached at ca. 100 min. Furthermore, the color of the XO and MB solutions gradually became lighter with the adsorption time. The color of the XO solution completely disappeared after the adsorption process. Accordingly, the PEI-TORC membrane shifted from dark red to orange after adsorption, in line with the dye removal efficiency results. In the adsorption stage, the large number of hydrophilic hydroxyl, carboxyl and amino groups on the surface of the adsorbent resulted in electrostatic interactions that occurred upon rapid migration of the anionic XO or cationic MB dyes to the surface adsorption sites (i.e., $-\text{COOH}$ and $-\text{NH}_2$) on the bioadsorbent, and the number of dye molecules adsorbed on the membrane increased with the adsorption time and levelled off at 50 min as a result of electrostatic repulsion forces between the adsorbed dye molecules. Therefore, the optimum contact time for the adsorption of XO and MB was ca. 50 min (i.e., 93% of XO and 83% of MB were removed). These results demonstrated that the PEI-TORC membrane is a good adsorbent for the rapid removal of XO and MB from waste waters.

As shown in Table 3, the R^2 values for MB and XO indicated that pseudo-second order (PSO) kinetic models could be used to predict the behavior over the whole range of the adsorption process, which indicating that the intraparticle diffusion was involved in the adsorption process. At a pH of 6.8, the q_e values for XO and MB calculated with a pseudo-second order model were 25 and 22 $\text{mg}\cdot\text{g}^{-1}$, respectively, and these values changed to 25 and 18 $\text{mg}\cdot\text{g}^{-1}$ at a pH of 4.6. These results were in good agreement with the experimental data.

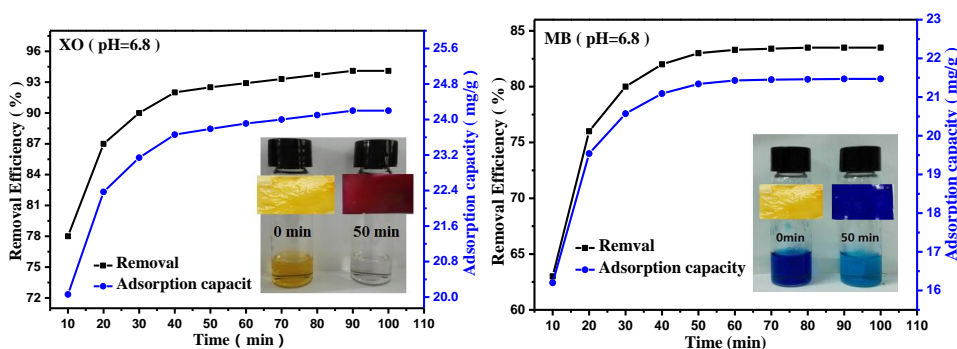


Figure 7. Cont.

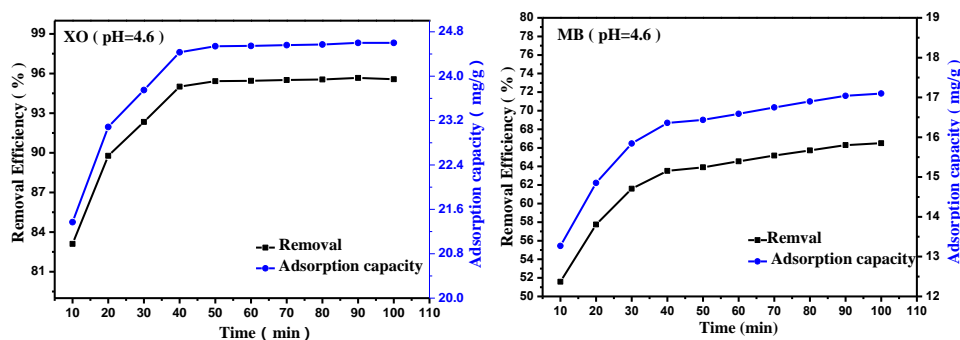


Figure 7. Effect of contact time on the dye removal efficiencies of XO and MB (initial dye concentration: 30 mg L^{-1} , 60 mL MB or XO solution, 70 mg adsorbent, 10–100 min, pH = 6.8 or 4.6).

Table 3. Kinetic parameters for the adsorption of XO and MB onto PEI-TORC.

pH	Dyes	Pseudo-First Order Model			Pseudo-Second Order Model		
		K_1 ($\text{g}\cdot\text{mg}^{-1}\cdot\text{min}^{-1}$)	q_e ($\text{mg}\cdot\text{g}^{-1}$)	R^2	K_2 ($\text{g}\cdot\text{mg}^{-1}\cdot\text{min}^{-1}$)	q_e ($\text{mg}\cdot\text{g}^{-1}$)	R^2
6.8	XO	0.049	5.16	0.9753	0.0092	24.75	0.9999
	MB	0.092	13.01	0.9954	0.017	22.16	0.9996
4.6	XO	0.072	5.09	0.9144	0.028	25.03	0.9999
	MB	0.054	7.61	0.9631	0.014	17.84	0.9997

3.6. Reusability

Figure 8 shows the reusability of the PEI-TORC membrane. After three consecutive desorption-adsorption cycles, the dye removal rates towards XO and MB decreased by 6 and 11%, respectively. Therefore, the adsorbent showed high reusability for the removal of XO and MB.

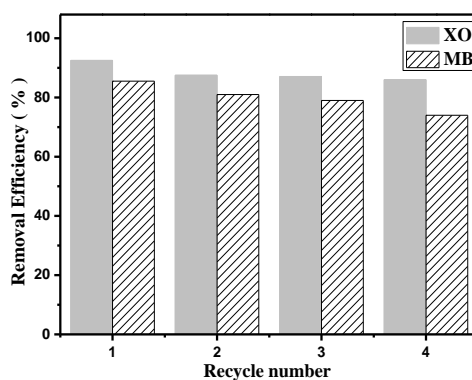


Figure 8. The dye removal efficiency of XO and MB after three desorption-adsorption cycles.

4. Conclusions

Functional membranes based on regenerated cellulose were prepared by grafting PEI onto controlled oxidized RC membranes. Modification conditions were screened to achieve the biofunctionalization of the regenerated cellulose membranes successfully and to retain the porous membrane structure. The maximum adsorption capacities of cationic and anionic dyes was observed, being the highest for xylenol orange ($403 \text{ mg}\cdot\text{g}^{-1}$), followed by methylene blue ($139 \text{ mg}\cdot\text{g}^{-1}$). Furthermore, the membranes showed low flux, supporting the usefulness of them as adsorbents. One may adjust the morphology, structure and properties of the PEI-TORC membrane by changing the various influencing factors in the preparation process, for exploring its potential application in the future.

Acknowledgments: Financial support from MOE&SAFEA for the 111 Project (B13025) is gratefully acknowledged.

Author Contributions: Wei Wang, Qian Bai, Huiyu Bai and Xiaoya Liu conceived of and designed the experiments. Wei Wang and Qian Bai performed the experiments and analyzed the data. Wei Wang, Qian Bai and Tao Liang wrote the paper. All authors discussed the results and improved the final text of the paper.

Conflicts of Interest: The authors declare no conflict of interest.

References

1. Sokolowska-Gajda, J.; Freeman, H.S.; Reife, A. Synthetic dyes based on environmental considerations. Part 2: Iron complexes formazan dyes. *Dyes Pigment.* **1996**, *30*, 1–20. [[CrossRef](#)]
2. Fleischmann, C.; Lievenbrück, M.; Ritter, H. Polymers and Dyes: Developments and Applications. *Polymers* **2015**, *7*, 717–746. [[CrossRef](#)]
3. Karadağ, E.; Saraydin, D.; Güven, O. Removal of some cationic dyes from aqueous solutions by acrylamide/itaconic acid hydrogels. *Water Air Soil Pollut.* **1998**, *106*, 369–378. [[CrossRef](#)]
4. Sharma, P.; Kaur, H.; Sharm, M.; Sahore, V. A review on applicability of naturally available adsorbents for the removal of hazardous dyes from aqueous waste. *Environ. Monit. Assess.* **2011**, *183*, 151–195. [[CrossRef](#)] [[PubMed](#)]
5. Liu, L.L.; Yu, C.X.; Zhou, W.; Zhang, Q.G.; Liu, S.M.; Shi, Y.F. Construction of Four Zn(II) Coordination Polymers Used as Catalysts for the Photodegradation of Organic Dyes in Water. *Polymers* **2016**, *8*, 3. [[CrossRef](#)]
6. Guendouz, S.; Khellaf, N.; Zerdaoui, M.; Ouchefoun, M. Biosorption of synthetic dyes (direct red 89 and reactive green 12) as an ecological refining step in textile effluent treatment. *Environ. Sci. Pollut. Res.* **2013**, *20*, 3822–3829. [[CrossRef](#)] [[PubMed](#)]
7. Ganesan, P.; Kamaraj, R.; Sozhan, G.; Vasudevan, S. Oxidized multiwalled carbon nanotubes as adsorbent for the removal of manganese from aqueous solution. *Environ. Sci. Pollut. Res.* **2013**, *20*, 987–996. [[CrossRef](#)] [[PubMed](#)]
8. Sanghi, R.; Bhattacharya, B. Review on decolorisation of aqueous dye solutions by low cost adsorbents. *Color Technol.* **2002**, *118*, 256–269. [[CrossRef](#)]
9. Kyzas, G.; Kostoglou, M. Green Adsorbents for Wastewaters: A Critical Review. *Materials* **2014**, *7*, 333–364. [[CrossRef](#)] [[PubMed](#)]
10. Zhou, Y.; Zhang, M.; Hu, X.; Wang, X.; Niu, J.; Ma, T. Adsorption of Cationic Dyes on a Cellulose-Based Multicarboxyl Adsorbent. *J. Chem. Eng. Data* **2013**, *58*, 413–421. [[CrossRef](#)]
11. Jin, L.; Li, W.; Xu, Q. Amino-functionalized nanocrystalline cellulose as an adsorbent for anionic dyes. *Cellulose* **2015**, *22*, 2443–2456. [[CrossRef](#)]
12. Qiao, H.; Zhou, Y.; Yu, F.; Wang, E.; Min, Y.; Huang, Q.; Pang, L.; Ma, T. Effective removal of cationic dyes using carboxylate-functionalized cellulose nanocrystals. *Chemosphere* **2015**, *141*, 297–303. [[CrossRef](#)] [[PubMed](#)]
13. Qi, Y.; Li, J.; Wang, L. Removal of Remazol Turquoise Blue G-133 from aqueous medium using functionalized cellulose from recycled newspaper fiber. *Ind. Crop. Prod.* **2013**, *50*, 15–22. [[CrossRef](#)]
14. Luo, X.G.; Zhang, L. High effective adsorption of organic dyes on magnetic cellulose beads entrapping activated carbon. *J. Hazard. Mater.* **2009**, *171*, 340–347. [[CrossRef](#)] [[PubMed](#)]
15. Shiralipour, R.; Larki, A. Pre-concentration and determination of tartrazine dye from aqueous solutions using modified cellulose nanosponges. *Ecotoxicol. Environ. Saf.* **2017**, *135*, 123–129. [[CrossRef](#)] [[PubMed](#)]
16. Zhu, W.; Liu, L.; Liao, Q.; Chen, X.; Qian, Z.; Shen, J.; Liang, J.; Yao, J. Functionalization of cellulose with hyperbranched polyethylenimine for selective dye adsorption and separation. *Cellulose* **2016**, *23*, 3785–3797. [[CrossRef](#)]
17. Ma, H.; Burger, C.; Hsiao, B.S.; Chu, B. Nanofibrous microfiltration membrane based on cellulose nanowhiskers. *Biomacromolecules* **2012**, *13*, 180–186. [[CrossRef](#)] [[PubMed](#)]
18. Karim, Z.; Mathew, A.P.; Grahn, M.; Mouzon, J.; Oksman, K. Nanoporous membranes with cellulose nanocrystals as functional entity in chitosan: removal of dyes from water. *Carbohydr. Polym.* **2014**, *112*, 668–676. [[CrossRef](#)] [[PubMed](#)]

19. Gopakumar, D.A.; Pasquini, D.; Henrique, M.A.; Morais, L.C.; Grohens, Y.; Thomas, S. Meldrum's Acid Modified Cellulose Nanofiber-Based Polyvinylidene Fluoride Microfiltration Membrane for Dye Water Treatment and Nanoparticle Removal. *ACS Sustain. Chem. Eng.* **2017**, *5*, 2026–2033. [[CrossRef](#)]
20. Wang, K.; Ma, Q.; Wang, S.D.; Liu, H.; Zhang, S.Z.; Bao, W.; Zhang, R.Q.; Ling, L.Z. Electrospinning of silver nanoparticles loaded highly porous cellulose acetate nanofibrous membrane for treatment of dye wastewater. *Appl. Phys. A* **2016**, *122*, 40. [[CrossRef](#)]
21. Carpenter, A.W.; Lannoy, C.F.; Wiesner, M.R. Cellulose nanomaterials in water treatment technologies. *Environ. Sci. Technol.* **2015**, *49*, 5277–5287. [[CrossRef](#)] [[PubMed](#)]
22. He, S.; Fang, H.; Xu, X. Filtering absorption and visual detection of methylene blue by nitrated cellulose acetate membrane. *Korean J. Chem. Eng.* **2016**, *33*, 1472–1479. [[CrossRef](#)]
23. Oshima, T.; Kondo, K.; Ohto, K.; Inoue, K.; Baba, Y. Preparation of phosphorylated bacterial cellulose as an adsorbent for metal ions. *React. Funct. Polym.* **2008**, *68*, 376–383. [[CrossRef](#)]
24. Ma, X.J.; Cao, S.L.; Lin, L. Hydrothermal pretreatment of bamboo and cellulose degradation. *Bioresour. Technol.* **2013**, *148*, 408–413. [[CrossRef](#)] [[PubMed](#)]
25. Fitz-Binder, C.; Bechtold, T. One-sided surface modification of cellulose fabric by printing a modified TEMPO-mediated oxidant. *Carbohydr. Polym.* **2014**, *106*, 142–147. [[CrossRef](#)] [[PubMed](#)]
26. Sun, X.F.; Wang, S.G.; Cheng, W.; Fan, M.; Tian, B.H.; Gao, B.Y.; Li, X.M. Enhancement of acidic dye biosorption capacity on poly(ethylenimine) grafted anaerobic granular sludge. *J. Hazard. Mater.* **2011**, *189*, 27–33. [[CrossRef](#)] [[PubMed](#)]
27. Zhang, L.; Mao, Y.; Zhou, J.; Cai, J. Effects of Coagulation Conditions on the Properties of Regenerated Cellulose Films Prepared in NaOH/Urea Aqueous Solution. *Ind. Eng. Chem. Res.* **2005**, *44*, 522–529. [[CrossRef](#)]
28. Cai, J.; Wang, L.X.; Zhang, L.N. Influence of coagulation temperature on pore size and properties of cellulose membranes prepared from NaOH–urea aqueous solution. *Cellulose* **2007**, *14*, 205–215. [[CrossRef](#)]
29. Mohamed, M.A.; Salleh, W.N.W.; Jaafar, J.; Ismail, A.F.; Mutalib, M.A.; Jamil, S.M. Feasibility of recycled newspaper as cellulose source for regenerated cellulose membrane fabrication. *J. Appl. Polym. Sci.* **2015**, *132*, 43. [[CrossRef](#)]
30. Lai, C.; Guo, X.; Xiong, Z. A comprehensive investigation on adsorption of Ca (II), Cr (III) and Mg (II) ions by 3D porous nickel films. *J. Colloid Interface Sci.* **2016**, *463*, 154–163. [[CrossRef](#)] [[PubMed](#)]
31. Yu, X.; Tong, S.; Ge, M. Synthesis and characterization of multi-amino-functionalized cellulose for arsenic adsorption. *Carbohydr. Polym.* **2013**, *92*, 380–387. [[CrossRef](#)] [[PubMed](#)]
32. Montanari, S.; Roumani, M.; Heux, L.; Vignon, M.R. Topochemistry of Carboxylated Cellulose Nanocrystals Resulting from TEMPO-Mediated Oxidation. *Macromolecules* **2005**, *38*, 1665–1671. [[CrossRef](#)]
33. Han, K.N.; Yu, B.Y.; Kwak, S.Y. Hyperbranched poly (amidoamine)/polysulfone composite membranes for Cd (II) removal from water. *J. Membr. Sci.* **2012**, *396*, 83–91. [[CrossRef](#)]
34. Sehaqui, H.; Larraya, U.P.D.; Liu, P.; Pfenninger, N.; Mathew, A.P. Enhancing adsorption of heavy metal ions onto biobased nanofibers from waste pulp residues for application in wastewater treatment. *Cellulose* **2014**, *21*, 2831–2844. [[CrossRef](#)]
35. Khan, M.N.; Bhutto, S. Kinetic study of the oxidative decolorization of xylene orange by hydrogen peroxide in micellar medium. *JCCS* **2010**, *55*, 170–175.
36. Zhang, W.; Zhou, C.; Zhou, W.; Lei, A.; Zhang, Q.; Wan, Q.; Zou, B. Fast and Considerable Adsorption of Methylene Blue Dye onto Graphene Oxide. *Bull. Environ. Contam. Toxicol.* **2011**, *87*, 86–90. [[CrossRef](#)] [[PubMed](#)]
37. Chen, C.; Zhang, M.; Guan, Q. Kinetic and thermodynamic studies on the adsorption of xylene orange onto MIL-101 (Cr). *Chem. Eng. J.* **2012**, *183*, 60–67. [[CrossRef](#)]
38. Min, L.U.; Zhang, Y.; Guan, X. Thermodynamics and kinetics of adsorption for heavy metal ions from aqueous solutions onto surface amino-bacterial cellulose. *Trans. Nonferrous Met. Soc.* **2014**, *24*, 1912–1917.

